The Monte Carlo Method: Versatility Unbounded in a Dynamic Computing World
Chattanooga, Tennessee, April 17-21, 2005, on CD-ROM, American Nuclear Society, LaGrange Park, IL (2005)

A NEW FACILITY FOR MCNP APPLICATION IN WHOLE BODY COUNTING AND INTERNAL DOSIMETRY

N. Borisov
State Research Center — Institute of Biophysics
46, Zhivopisnaya St., Moscow, 123182 Russia;
Institut de Radioprotection et de Sûreté Nucléaire
B.P. 17, Fontenay-aux Roses Cedex, 92262 France
borisov@srcibph.ru; nikolay.borisov@jefferson.edu

D. Franck, L. de Carlan, N. Pierrat
Institut de Radioprotection et de Sûreté Nucléaire
B.P. 17, Fontenay-aux Roses Cedex, 92262 France
didier.franck@irsn.fr; loic.decarlan@irsn.fr; noelle.pierrat@irsn.fr

O. Kochetkov, V. Yatsenko
State Research Center — Institute of Biophysics
46, Zhivopisnaya St., Moscow, 123182 Russia
kochetkov@srcibph.ru; yatsenko@srcibph.ru

ABSTRACT

Development of precision measurement techniques (such as whole body spectrometry), as well as techniques for processing the results of such measurements, opens an opportunity to increase essentially the reliability of internal irradiation monitoring of nuclear industry personnel. The major difficulties of such monitoring are related to measurements of low-energy γ-radiation which is intensively absorbed and scattered in body tissues (e.g., for such biologically important radionuclides, as ^{239}Pu and ^{241}Am). The attenuation of radiation depends on individual anatomy of a patient. Such individual anatomy cannot be taken into account correctly when using plastic phantoms (mannequins) for calibration of whole body spectrometers. On the contrary, calculations can provide adequate representation of the individual if radiation transport is simulated in voxel geometry retrieved from medical tomography images. For such calculations, only Monte Carlo method can be used in practice. The paper reviews a recently developed graphical user interface for automatic creation of MCNP input data files. The voxel geometry of radiation transport is restored on the base of the patient's tomograms. The new software enables also graphical analysis of calculation results. The GUI was successfully used for whole body counter calibration as well for studies of influence of individual anatomical features on counting efficiency of whole body spectrometers. The accurate description of the patients anatomy provided by the utility allows correction of interpretation of the measured date by at least of a two-fold factor. The new technique seems rather important for radiation monitoring of nuclear industry personnel.

Key Words: whole body counting; internal dosimetry; professional irradiation; MCNP; voxel phantom

1 INTRODUCTION

The radiation safety of atomic industry personnel handling transuranium radionuclides, ^{241}Am, ^{239}Pu etc., inevitably involves radiation monitoring and internal exposure control. The specialized techniques of individual monitoring used at atomic enterprises include the application of dynamic air concentration assessment in the working room air, daily sampling of human excreta and whole body counting spectrometry. This technique (which uses high-purity germanium detectors) is valued by numerous advantages. Among such advantages are the possibility of dynamic *in vivo* measurements of incorporated activity, high counting efficiency within wide energy range, high resolution for absorbed energy.

On the other hand, whole body counting has several disadvantages as well. The most crucial disadvantage is the need for interpretation of the measurement, i.e. determination of incorporated activity which corresponds to the number of pulses in spectrometry channels. To obtain the recalculation coefficients from number of pulses into radionuclide activity, plastic phantoms (mannequins) with reference activity are generally used. However, the standard reference phantoms do not take into account the individual anatomy of a given patient, the specific size, shape, weight of his (her) organs as well as their placement in the body. To make the things worse, the most biologically significant incorporated radionuclides (like ^{239}Pu and ^{241}Am) emit low-energy (13-60 keV) γ-rays. As a result, determination of whole body counting calibration coefficients is hampered due to intensive absorption and scattering of radiation in the patient's body.

To circumvent these obstacles, one could use mathematical simulation (particularly Monte Carlo method as almost the only valid calculation method for such a purpose) rather than measurement of reference phantoms. However, such calculations require an adequate model of the patient's anatomy. An anatomy model could be created either in terms of standard bodies limited by standard surfaces or in terms of small rectangular boxes (voxels) with certain density and chemical composition. These two opposite approaches both have several advantages and disadvantages. The advantage of the first approach (see, for instance, [1]) is mostly the simplicity of anatomy description that accelerates the calculations. However, this description could not be exact. On the contrary, the voxel approach (presented in, e.g., [2]) allows to describe precisely the individual patient anatomy, but requires significant resources of computer memory and run-time for transport calculations. As a result, the first approach is generally used for hygienic standardization (calculations of external exposure caused by high-energy radiation), whereas the second approach is more useful for calculations of internal exposure caused by low-energy radiation.

Until recent time, application of voxel approach to Monte Carlo calculations was essentially limited. Either low-resolution images [3, 4], or averaging through the neighbor voxles [2], or standard phantom libraries instead of individual phantoms [5, 6] were used. Due to progress of computer tomography (CT) methods, the reconstruction of voxel transport geometry based on CT seems very attractive for internal dosimetry.

The multi-platform (MS Windows and UNIX) graphic user interface ŒDIPE* [7] (formerly

*ŒDIPE is the abbreviation of a French phrase, "Outil d'Evaluation de la Dose Interne PErsonnalisée"

named *Anthropo*) developed at Institut de Radioprotection et de Sûreté Nucléaire (IRSN; Fontenay-aux-Roses, France) is specially designed for applications in internal dosimetry and whole body counting. To perform radiation transport calculations, the software ŒDIPE creates automatically MCNP [8] input data files retrieved from individual patient tomograms. Further graphic analysis of MCNP calculation results is also enabled.

The present paper overviews the major abilities of the ŒDIPE software on the examples of radiometry of plastic phantoms and arbitrary biological tissues as well as radiometry and internal dosimetry of a real patient.

2 THE SOFTWARE *ŒDIPE*

The software uses the following input data:

- magnetic resonance or x-ray tomograms of the patient's body;
- source description, i.e. source geometry (two options, point or distributed source, exist), as well as number of γ-quanta emitted and their energies, determined by radionuclide, source activity and measurement time;
- detector geometry and position regarding to the patient.

The ŒDIPE interface includes several service features for image processing, namely segmentation, erosion, dilatation, change of color and resolution, and margin trimming. The better results for segmentation of organs and tissues are achieved when processing the tomography images first with the DOSIGRAY software. Initially designed for radiotherapy planning in oncology, DOSIGDRAY allows organ and tissue separation in a grayscale image by plotting the contours of equal brightness. The ŒDIPE interface uses the contours obtained by DOSIGRAY software for segmentation of the image into organs and tissues. Segmentation according to pixel brightness of the grayscale image could be also done directly by ŒDIPE interface without image contouring by DOSIGRAY, although it is usually less convenient. After organ and tissue separation all the organs and tissues are assigned with their chemical composition and density, tabulated in ICRU Report 44 [9].

The MCNP input data file is automatically written by the ŒDIPE interface. It contains the information of the patient's body in voxel representation, detector materials and geometry (described in terms of standard surfaces rather than voxels), the tally of interest (pulse-height-spectrum of the detector or dose distribution inside the body). To accelerate the calculations, the neighbor voxels with the same density and chemical composition are coupled into larger rectangular boxes. To visualize the transport geometry written in the MCNP input data file, the Sabrina software is used [10].

The ŒDIPE interface includes also an additional module for graphic analysis of calculation results. According to the tally of interest, the module plots either pulse-height spectrum (both calculation and experimentally measured may be plotted in one window) or isodose curves and areas in cross sections of the patient's body.

The flexibility of the new software with respect to input data, particularly to the anatomy of an individual patient, allows the use of ŒDIPE for both internal dosimetry [11, 12] and whole

Table I: Experimental and calculated counting efficiency (for the Livermore phantom) in the photoelectric absorption peak of ^{241}Am (59.54 keV) for detectors placed in front of left and right lung

Detector	Calculation (C), s^{-1}·kBq^{-1}	Experiment (E), s^{-1}·kBq^{-1}	Difference, $D = ((C - E)/C) \cdot 100\%$
Left	0.85	0.78	$+9$
Right	1.41	1.55	-6

body counting spectrometry which is is described here.

3 COMPARISON OF EXPERIMENTAL AND CALCULATION DATA FOR WHOLE BODY COUNTING

The abilities of ŒDIPE for the problems of whole body counting were shown in the series of experiments and calculations with plastic human body phantoms and arbitrary samples of biological tissues (meat). During this checking procedures, good agreement was found between experimental and MCNP calculation data.

Several tests of the ŒDIPE utility were conducted at State Research Center — Institute of Biophysics (IBPh; Moscow, Russia) with the plastic torso phantom of the Livermore National Laboratory [13]. Perforated lungs of the phantoms contained 27 capsules with ^{241}Am. Total reference activity of the capsules was equal to 3165 Bq. The γ-radiation of ^{241}Am was measured with two low-energy germanium detectors manufactured by Canberra Industries, Inc. The detectors were placed at the "chest" of the phantom in front of the left and right lung.

To perform the mathematical simulation of these measurements, the Livermore phantom was scanned with the CT machine Toshiba Aquilion (image voxel number 256×256×51) at Clinical Hospital No. 6 of Federal Medico-Biological Agency of Russia (Moscow). The scanned image were processed with the ŒDIPE utility to generate the MCNP input data file (see Fig. 1). The ŒDIPE-made MCNP description of the phantom geometry keeps all the fine features of the plastic phantom (such as cavities, cracks, holes for capsules in lungs etc.) MCNP4c2 calculations for the phantom used the source term as multiple points; the point positions were determined by the capsule places in the CT images of the phantom.

The experimental and calculated spectra of whole body counters placed in front of left (panel "a") and right (panel "b") lung of the phantom are shown by Fig. 2. Table I contains counting efficiency data in the photoelectric absorption peak of ^{241}Am (59.54 keV) for right and left detector twins. Calculations did not use either counting efficiency correction versus the absorbed energy or spectrum normalization, so the calculated values of Fig. 2 and Table I are absolute ones rather than relative ones. The standard deviation in the maximum pulse counting channel for calculated spectrum is about 6% for 1 million histories of random tests, which requires about 20 minutes of calculation time at personal computer (3 GHz, 512 Mb RAM).

To test the ability of ŒDIPE to process the magnetic resonance images, several experiments

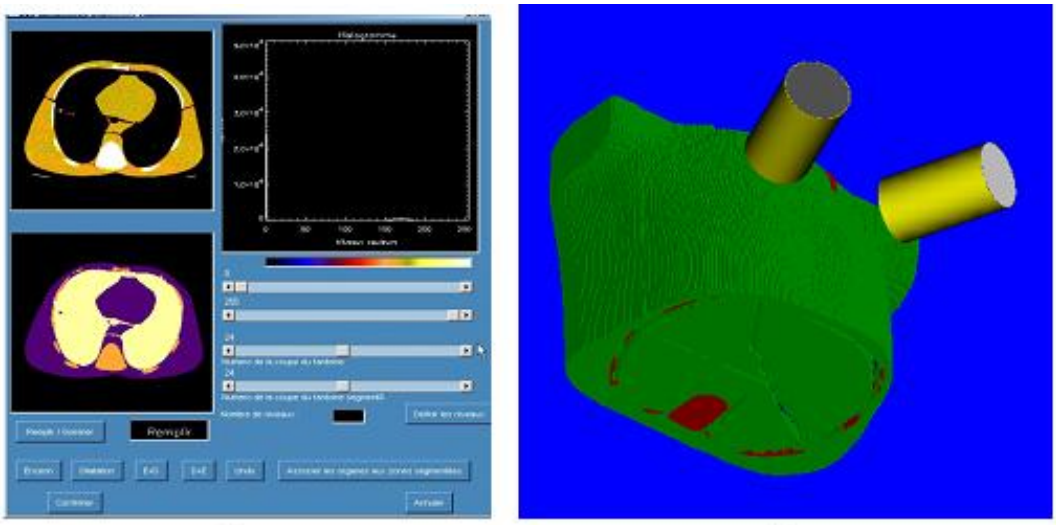

Figure 1: Processing of the Livermore phantom CT images whole body counting calibration. Panel "a": separation of organs and tissues applying ŒDIPE software. Left upper window: initial CT image and segmented image below (colors are related to the tissue types); right upper window: spectrum of initial image according to the pixel brightness. Panel "b": visualization of radiation transport geometry with Sabrina software. The transport geometry which was recorded by ŒDIPE software as MCNP input data file. The colors correspond to the type of the tissue or substance. Image voxel number: 256×256×51.

with arbitrary samples of biological tissues were conducted. Three meat samples (mouton knee, chicken body and a piece of beef) were scanned with the MRI tomography machine MAGNETOM at L'Hôpital d'Instructions des Armées Percy (Clamart, France). After MRI scanning the reference ^{241}Am source with activity of 32 kBq was placed inside the meat samples. The γ-radiation of ^{241}Am was measured with the low-energy germanium whole body counter Canberra Semiconductors at IRSN.

The visualized with ŒDIPE pulse-height-spectra (in counts per channel per second) for one of meat samples (mouton knee) shown in panel "a" of Fig. 3. The pink line indicates MCNP4c2 results whereas the red one indicates experimental. In the panel "b", there is a photo of the sample. The panel "c" presents Sabrina visualization of the MCNP input data file (including the detector). Several differences in the meat sample shape are explained by sample deformation inside MRI machine, which has a non-flat surface where the sample lay when being scanned. Table II contains the data on counting efficiency of the major photoelectric absorption peak for meat samples. Inside the limits of uncertainty caused by the unknown exact source placement inside the meat (which is particularly important for the chicken sample where the source was put inside the body cavity without any fixation), the calculated absolute intensity of full absorption peaks is close to the experimental one. The calculation time for DEC Alpha professional workstation depends on the complexity of the geometry. To achieve 1.5-2% for the standard

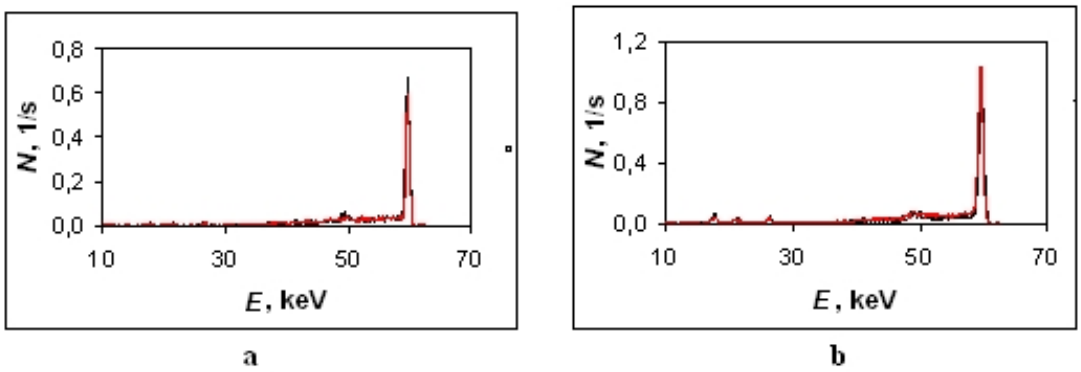

Figure 2: Experimental (red line) and calculated (black line) spectra of the left (panel "a") and right (panel "b") Canberra germanium detectors during measurement of γ-radiation emitted by ^{241}Am inserted into the lungs of the Livermore plastic phantom.

Table II: Experimental and calculated counting efficiency in the photoelectric absorption peak of ^{241}Am (59.54 keV) for meat measurement of samples

Sample	Calculation (C), s^{-1}·kBq^{-1}	Experiment (E), s^{-1}·kBq^{-1}	Difference, $D = ((C - E)/C) \cdot 100\%$
Mouton	6.50	7.13	-16
Chicken	5.84	4.13	$+30$
Beef	17.8	16.4	$+8$

deviation in the maximum spectrometry channel, which is possible after one million of statistic histories, one should spend from 3.50 min (beef sample) up to 17.30 min (chicken sample).

4 INTERCALIBRATION OF PHYSICAL PHANTOMS USED IN RADIATION HYGIENE

ŒDIPE was also used for testing the adequacy of physical phantoms for representation of a certain patient's anatomy during the measurements with whole body counters [15]. Several phantoms used in radiation hygiene (the Livermore phantom, the JAERI torso phantom, the full body RANDO phantom and the Winfrith Technology Centre hollow phantom filled with tissue-equivalent granules) were scanned with the x-ray CT machine at L'Hôpital Percy. One of the patients of the same hospital was used as reference and was also scanned with the same tomography machine. To fit the anatomy of the patient, the Livermore phantom was used with the plate No. 3 (series B), and the JAERI phantom with the 3.6 cm thick plate. The images of the phantoms and the patient segmented with ŒDIPE as well as the general views of the phantoms are shown in Fig. 4. The slices displayed correspond to the middle of the lungs along the vertical axis. The central axis of the detector was placed within the slices displayed. The description of the phantoms is given in ICRU Report 48 [14]. Their major features are listed by Table III. The

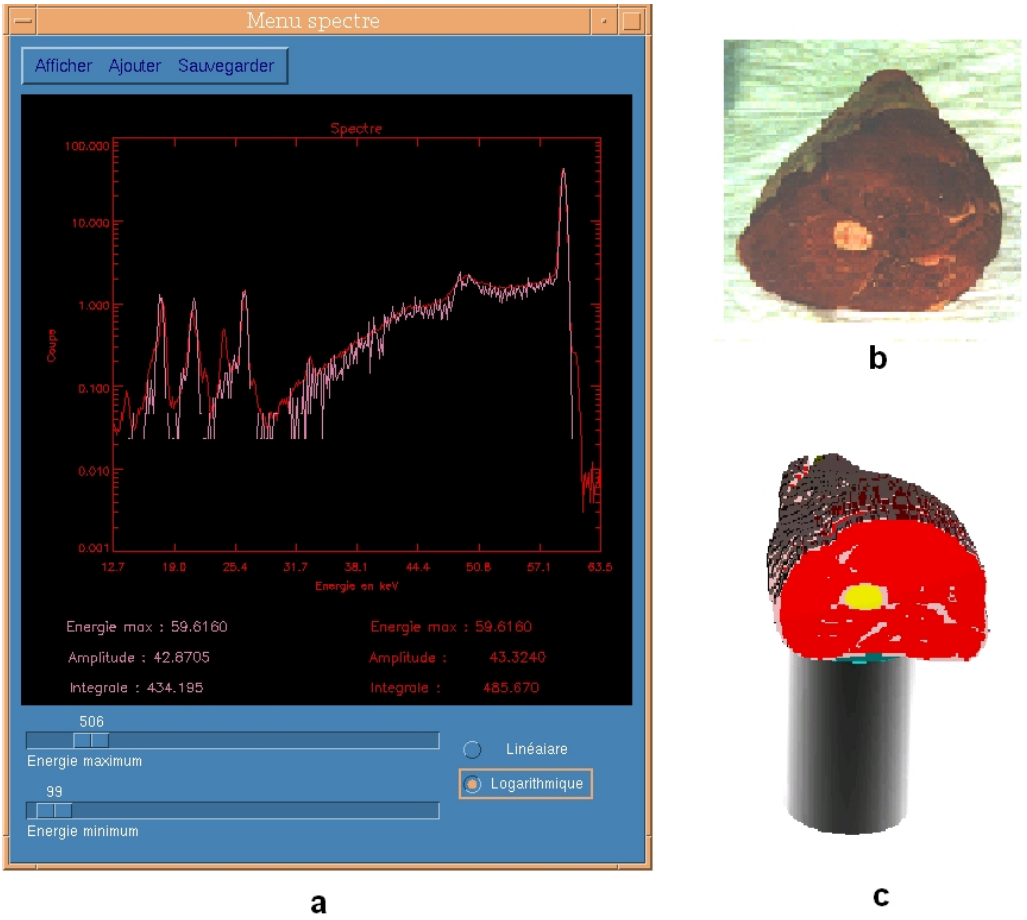

Figure 3: Panel "a": experimental (red line) and calculated (pink line) pulse-height-spectra from point ^{241}Am source of 32 kBq, placed into mouton meat sample counts per second per channel. Panel "b": photo of the sample. Panel "c" – Sabrina visualization of MCNP geometry (including the detector), created by ŒDIPE.

principal distances $L_{\min}$ and $L_{\max}$ (see also explanation in Fig. 5) from Table III are obtained via averaging distance from the closest point of the lungs to the detector within the slice displayed in Fig. 4 and four points on the lung surface surrounding the closest point at the radius of 1 cm. During images processing with DOSIGRAY and ŒDIPE, to provide the uniformity of calculations, and to study the influence of pure geometry parameters on phantom calibration, muscle and fat tissues were not distinguished for all of the phantoms and the patient (all soft tissues were assigned as "muscle"). When converting phantom images to MCNP geometry, all small details (cracks, cavities etc.) were taken into account.

The counting efficiency calculated with MCNP4c2 for the phantoms was compared with the same efficiency for the patient. The calculations were done for low-energy germanium γ-ray detector (LEGe) placed in front of the right lung (see also Fig. 5). In the calculations the activity was considered to be uniformly distributed through the lungs. The relative difference in calculated

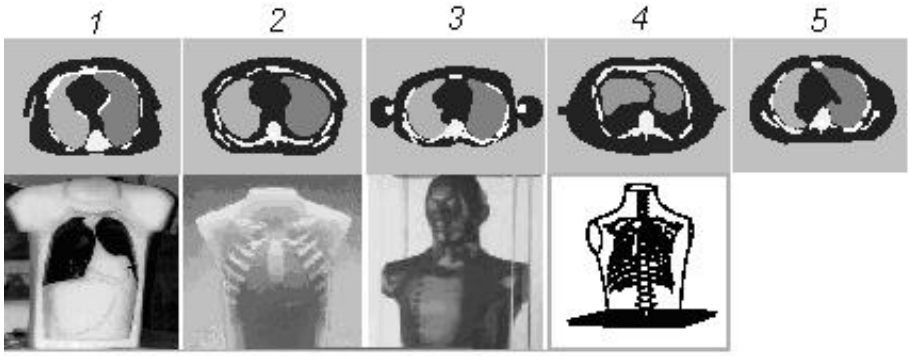

Figure 4: The upper row: Tomograms of the Livermore phantom (1), the JAERI phantom (2), the RANDO phantom (3), the Winfrith phantom (4) as well as of a L'Hôpital Percy patient segmented by DOSIGRAY and ŒDIPE. The lower row: general view of the phantoms 1-4, respectively.

counting efficiency for phantoms and the patient (the result for a phantom minus the result for the patient, divided by the result for the patient), is shown in Fig. 6. The calculations were made for the most important energies of γ-rays emitted by ^{241}Am (13.9, 17.54, 21.01, 26.35 and 59.54 keV) and ^{235}U (15.50, 89.90, 93.30, 105.00, 109.16, 143.76, 163.33, 185.72 205.31 keV). The length of error bar in Fig. 6 corresponds to one standard deviation for Monte Carlo method. The difference in counting efficiency (which may be as high as 50% and more for energies lower then 50 keV) is caused by the difference in anthropometric data of phantoms and the patient.

Considering the phantoms mentioned in this paper, the worst patient anatomy representation is provided by the Winfrith phantom, which has extremely small lungs, shifted to anterior direction along anterior-posterior axis. Rather thick chest wall, related to $L_{\min}$ parameter (see Table III), causes intensive absorption in low-energy range, where ratio of counting efficiency for the phantom and the patient is quickly decreasing when energy decreases (see Fig. 6). However, lungs in the Winfrith phantom are abnormally shifted to the front part of chest, which makes not only maximal distance $L_{\max}$, but also median distance L_{med}, shorter for the Winfrith phantom than for the patient. As a result, it provides a "compensation" of absorption for higher energies, which explains the apparent closeness of the patient and the Winfrith phantom in the 100-200 keV range.

The RANDO phantom lungs are also smaller and more deeply located in comparison to the patient (about 1 cm of shift for the three L parameters). As a result, in all the energy range counting efficiency is lower for the RANDO phantom than for the patient over the entire energy range.

The lungs of the Livermore phantom are more extended along anterior-posterior direction than for the patient (see Fig. 4). One the contrary, the lungs of the JAERI phantom are less extended along this direction in comparison to the patient. This provides higher efficiency for energies lower than 30 keV for the Livermore phantom than for the JAERI phantom, caused by longer $L_{\min}$ of the latter. In this energy range one can observe that efficiency for the Livermore phantom is almost equal to that for the patient. Contrary, longer $L_{\max}$ and L_{med} for the Livermore

Table III: Major features of the scanned phantoms

	Livermore Plate No. 3	JAERI with plate	RANDO	Winfrith	Patient
Whole body height, cm	177	168	175	175	Non available
Whole body weight, kg	76	63.5	73.5	72.5	74.5
Thickness of front soft tissue layer, $L_{\min}$, cm	3.6	3.7	4.3	3.8	3.0
Depth of back lung boundary, $L_{\max}$, cm	23.9	17.1	19.5	13.8	19.2
Median distance to the lungs, $L_{\mathrm{med}} = (L_{\min} + L_{\max})/2$, cm	13.7	10.4	11.9	8.9	11.1
Right lung volume, cm^3	2294	2002	1855	768	1849
Left lung volume, cm^3	1781	1689	1581	815	1292

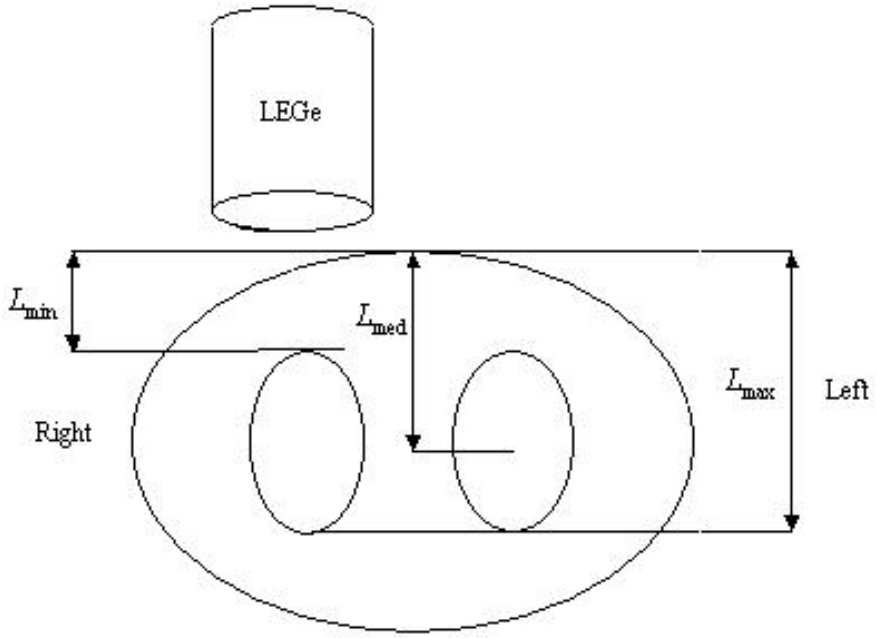

Figure 5: Scheme of principal distances from lungs to the front surface of thorax during whole body counting with low-energy germanium detector (LEGe). $L_{\min}$ is the minimal distance between source (lung) and front surface, it determines counting efficiency for low energies. For higher energies, maximal distance $L_{\max}$ and median L_{med} are also essential.

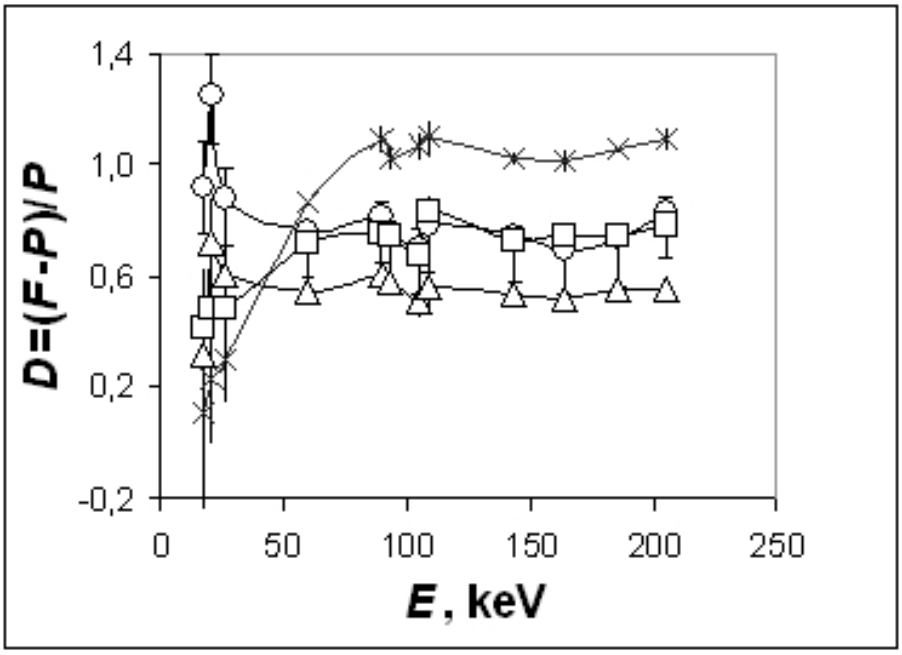

Figure 6: Relative calculated counting efficiency for ^{241}Am and ^{235}U photoelectric absorption peaks for phantoms and the patient, $D = (F - P)/P$, where F is the result for a phantom and P is the result for the patient. ◯ — the Livermore phantom, □ — the JAERI phantom, △ — the RANDO phantom, × — the Winfrith phantom.

phantom than for the JAERI phantom provides additional absorption for the former in energy range 50-200 keV. As a result, counting efficiencies the Livermore and JAERI phantoms for such energies are almost equal, but they are 30% lower than for the patient.

5 CONCLUSION

Recent studies in calculation methods for internal dosimetry and *in vivo*-radiometry have been focused on application of individual voxel phantoms for Monte Carlo radiation transport simulation. The voxel phantom approach allows taking into account the individual features of the patient's anatomy, which is particularly important for β- and low-energy γ-exposure. However, it requires considerable resources of calculation time and computer memory as well as considerable effort for input data file preparation.

To facilitate the use of individual voxel phantoms during Monte Carlo calculations, a new multi-platform graphic user interface has been developed. This software processes the x-ray or magnetic resonance computer tomography images of an individual patient to convert them into MCNP geometry description in terms of voxels. To reduce MCNP calculation time, the neighbor voxels with the same density and chemical composition are coupled into larger rectangular boxes. The tools for the source and detector description as well as for output file graphical analysis are also included to the software.

The validity of the new software has been tested for low-energy γ-ray spectrometry of actinides when measuring plastic phantoms and arbitrary samples of biological tissues. The interface proves to be useful for whole body counting calibration where the influence of a calibration phantom to the interpretation of the measured data has been studied. The software enables taking into account individual patient's anatomy, which may result in up to two-fold and more correction factors for activity assessment.

The software also enables the use of MCNP calculation of spatial dose distribution in voxel phantom geometry [11, 12]. The application of the new utility for dose monitoring of nuclear industry personnel seems to be attractive.

6 ACKNOWLEDGMENTS

The authors warmly appreciate the assistance of Service d'Imagerie Médicale at L'Hôpital d'Instruction des Armées Percy (Clamart, France) and its head, D. Jeanbourquin, who provided MRI scanning of meat samples and x-ray CT scanning of anthropomorphic plastic phantoms.

The assisatance of Computer Tomography Department of Clinical Hospital No. 6 of Federal Medico-Biological Agency (Moscow, Russia), especially its head, L. B. Tumanov, and its principal specialist, T. Ts. Tsedish, who provided x-ray CT scanning of the Livermore phantom with perforated lungs, is equally appreciated.

Special thanks should also be addressed to J. L. Genicot from Belgian Nuclear Research Center, (SCK CEN; Mol, Belgium), who provided the Winfrith phantom for CT scanning and intercalibration.

Part of the work was supported by the Partnership IBPh-IRSN Project No. 2699 under the egide of International Science and Technology Center (ISTC).

7 REFERENCES

1. M. Christy, K. Eckerman. "Specific Absorbed Fraction of Energy at Varios Ages from Internal Photon Sources," ORNL/TM-8381/V1 (1987).
2. M. Mallett, B. Hickman, D. Kruchten, J. Poston. "Development of a Method for Calibrating *in vivo* Measurement Systems Using Magnetic Resonance Imaging and Monte Carlo Calculations," *Health Physics,* **68**, pp. 773-785 (1995).
3. T. Ishikawa, M. Uchiyama. "Calculation of the Counting Efficiency for ^{137}Cs Using Voxel Phantom with Lungs and a Skeleton," *Radiation Protection & Dosimetry,* **69**, pp. 199-204 (1997).
4. T. Ishikawa, M. Uchiyama. "Estimation of the Counting Efficiencies for Individual Subjects in ^{137}Cs Whole-Body Counting Using Voxel Phantoms," *Radiation Protection & Dosimetry,* **71**, pp. 195-200 (1997).
5. D. Hickman, M. Firpo. "Magnetic Resonance Image Phantom Program," UCRL-MA-118455 (1997).

6. J. Hunt, I. Malatova, S. Foltanova, B. Dantas. “Calibration of *in vivo* Measurement System Using a Voxel Phantom and the Monte Carlo Technique,” *Radiation Protection & Dosimetry,* **89**, pp. 283-286 (2000).
7. N. Borisov, D. Franck, L. Laval, L. de Carlan. “A New Graphical Usr Interface for Fast Construction of Computation Phantoms and MCNP Calculations: Application to Calibration of *in vivo* Measurement Systems,” *Health Physics,* **83**, pp. 272-280 (2002).
8. J. Briesmeister. “MCNP — A general Monte Carlo N-particle Transport Code, version 4c,” LA-13709-M (2000).
9. “International Commission on Radiation Units and Measurements. Tissue Substitutes in Radiation Dosimetry and Measurements,” ICRU Report 44, Bethesda, MD (1989).
10. A. V. Kenneth. “Users Guide for Sabrina. Version 3.56, Radiation Transport Group – Applied Theoretical Physics Division, Los Alamos National Laboratory,” LA-UR-93-3696 (1994).
11. L. de Carlan, I. Aubineau-Lanièce, A. Lemosquet, N. Borissov, J.-R. Jourdain, D. Jeanbourquin, B. Le Guen, D. Franck. “Application of New Imaging and Calculation Techniques to Activity and Dose Assessment in the Case of a ^{106}Ru Contaminated Wound,” *Radiation Protection & Dosimetry,* **105**, pp. 219-223 (2003).
12. I. Aubineau-Lanièce, L. de Carlan, D. Franck, S. Chiavassa, M. Bardiès. “Experience at IRSN on Voxel Phantoms for Internal Dosimetry using a Dedicated Computational Tool,” *The Monte Carlo Method: Versatility Unbounded in a Dynamic Computing World,* Chattanooga, Tennessee, April 17-21, 2005, on CD-ROM, American Nuclear Society, LaGrange Park, IL (2005).
13. R. V. Griffith, P. N. Dean, A. L. Anderson, J. C. Fisher. “A Tissue-Equivalent Torso Phantom for Intercalibration of *in vivo* Transuranic Nuclide Counting Facilities,” *Advances in Radiation Protection Monitoring,* pp. 493-504, IAEA 44, Stockholm, Sweden, (1978).
14. “International Commission on Radiation Units and Measurements. Phantoms and Computational Models in Therapy, Diagnosis and Protection,” ICRU Report 48, Bethesda, MD (1992).
15. D. Franck, N. Borissov, L. de Carlan, N. Pierrat, J.-L. Genicot, G. Etherington. “Application of Monte Carlo Calculations to Calibration of Anthropomorphic Phantoms Used for Activity Assessment of Actinides in Lungs,” *Radiation Protection & Dosimetry,* **105**, pp. 403-408 (2003).